






Forced Motion Activated Self-Alignment of Micro-CPV Solar Cells

Elisa Kaiser , Maike Wiesenfarth , Victor Vareilles , Martin Schneider-Ramelow, Stefan W. Glunz , *Senior Member, IEEE*, and Henning Helmers , *Senior Member, IEEE*

Abstract—In micro-concentrating photovoltaics (micro-CPV), the size of solar cells is reduced ($<1 \times 1 \text{ mm}^2$) compared to conventional CPV. However, the quantity and requirement for placement accuracy of solar cells is increased. To be economically competitive, a promising possibility for the die assembly is a high throughput and relatively unprecise pick and place process combined with surface tension-driven self-alignment of the liquid solder. In this article, this approach is experimentally investigated, with a focus on the influences of solder volume, receiving pad layouts, and initial displacements of the cells on the self-alignment accuracy. Here, we show that an induced motion due to the initial displacement of the cells or due to solder flow along tracks leads to a more robust and accurate process. We found that less solder and rather smaller pads than cells (here by $92 \text{ }\mu\text{m}$ or 10.4% of the cell length) are beneficial for self-alignment accuracy. However, for micro-CPV, conductor tracks connected to the pad are required for electrical interconnection and heat dissipation. Here, all cells are self-aligned and reach an accuracy between -15 and $+15 \text{ }\mu\text{m}$, which is mainly due to the cell-to-pad size difference. Optical simulations show that this displacement would lead to an optical loss of 0.1%_{abs} instead of 12.1%_{abs} when displacing the cell by $150 \text{ }\mu\text{m}$. Thus, the self-alignment using the surface tension of the liquid solder leads to sufficient accuracy.

Index Terms—III-V, micro-concentrating photovoltaic (micro-CPV), module manufacturing, pad layout, self-alignment, solar cell alignment, solder volume, surface tension.

I. INTRODUCTION

MICRO-CONCENTRATING photovoltaics (micro-CPV), the miniaturization of solar cell size to below

Manuscript received 10 October 2023; accepted 3 January 2024. Date of publication 29 January 2024; date of current version 20 February 2024. This work was supported in part by the German Federal Ministry for Economic Affairs and Climate Action (BMWK) under the “micro-CPV” project (#03EE1046A) and in part by the Institut Carnot Energies du Futur in the framework of the PV μ Co project. (*Corresponding author: Elisa Kaiser.*)

Elisa Kaiser and Stefan W. Glunz are with the University of Freiburg, 79098 Freiburg, Germany, and also with the Fraunhofer Institute for Solar Energy Systems ISE, 79110 Freiburg, Germany (e-mail: elisa.kaiser@ise.fraunhofer.de; stefan.glunz@ise.fraunhofer.de).

Maike Wiesenfarth and Henning Helmers are with the Fraunhofer Institute for Solar Energy Systems ISE, 79110 Freiburg, Germany (e-mail: maike.wiesenfarth@ise.fraunhofer.de; henning.helmerts@ise.fraunhofer.de).

Victor Vareilles is with University Grenoble Alpes, CEA-Liten, INES, 73375 Le Bourget du Lac, France, and also with University Lyon, CNRS, INSA Lyon, ECL, UCBL, CPE Lyon, INL, UMR5270, 69621 Villeurbanne, France (e-mail: victor.vareilles@cea.fr).

Martin Schneider-Ramelow is with the Technical University of Berlin, 13355 Berlin, Germany (e-mail: martin.schneider-ramelow@tu-berlin.de).

Color versions of one or more figures in this article are available at <https://doi.org/10.1109/JPHOTOV.2024.3355403>.

Digital Object Identifier 10.1109/JPHOTOV.2024.3355403

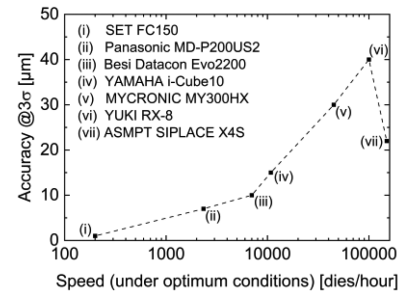


Fig. 1. Die placement accuracy dependent on speed for different commercial pick-and-place machines.

1 mm^2 , is one major trend in CPV [1], [2], [3]. The reduction of the component sizes leads to a lower heat load per solar cell. Hence, otherwise required heat spreaders can be omitted and low-cost printed circuit board (PCB) technology can be applied. Typically, PCB on glass is used to match the coefficient of thermal expansion of the also glass-based lens plate; in addition, it yields good mechanical and long-term stability. To assemble the increased number of solar cells, parallelized and/or high throughput processes from other industries, such as panel level packaging in micro- and optoelectronics, micro-/mini-light-emitting diode (LED) display technology and advanced PCB technologies (chip-on-board and chip-on-glass), can be adapted and promise cost-reduction for CPV. Various micro-CPV module approaches have been presented with micro-scale solar cells with edge lengths below 1 mm , e.g., [4], [5], [6], [7], [8], [9], [10].

Yet, the required precision regarding alignment of the solar cells with respect to the optics that comes with miniaturization poses a challenge: While offsets in the order of $50 \text{ }\mu\text{m}$ may be irrelevant for $5 \times 5 \text{ mm}^2$ devices, they are critical for $0.5 \times 0.5 \text{ mm}^2$ devices. To assemble these small devices, in industry, the current standard for precise die bonding is pick-and-place. The assembly rate depends on the machine speed, distances between chips, the number of assembly heads, and the required accuracy. Fig. 1 shows a survey of data sheet information of state-of-the-art pick-and-place machines. As can be seen in the graph, higher accuracy implies fewer dies per hour and, thus, higher related manufacturing costs. High speeds ($170\,000$ or $\sim 1\,000\,000$ dies/hour [11]) and high accuracies (up to $2 \text{ }\mu\text{m}$ [12] or $5 \text{ }\mu\text{m}$ [11]) are achievable with micro transfer printing, which however requires accurate stamps and sophisticated equipment. Fluidic self-assembly [13], [14] on the other hand, promises high

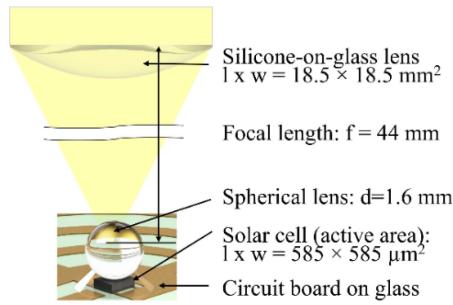


Fig. 2. Sketch of the micro-CPV module and its components.

speeds with comparatively imprecise tools, as the placement is done via a continuous fluidic flow or batch-wise in a fluid container. While the accurate positioning is achieved through surface tension driven self-alignment.

A sketch of our micro-CPV module design, developed at Fraunhofer ISE, is shown in Fig. 2. It is based on a circuit board on glass. $35 \mu\text{m}$ thick Cu tracks are used for electrical interconnection and heat dissipation. The cell temperatures during operation depends on the specific circuit board layout and has been estimated to be between 65°C and 85°C [15]; for solder layer thicknesses of $100 \mu\text{m}$ it has no significant influence on heat dissipation. Micro 5-junction (5j) concentrator solar cells [16] with an active area of $585 \times 585 \mu\text{m}^2$ and rectangular chip size of $885 \times 685 \mu\text{m}^2$ are used. The cells are soldered using a no-clean SnAgCu (SAC) paste and a reflow process. The front contact of the solar cell is wire bonded. All cells are equipped with spherical lenses with a diameter of 1.6 mm as secondary optical elements. The primary optical element is a silicone-on-glass plano-convex lens with an edge length of $18.5 \times 18.5 \text{ mm}^2$ and a focal distance of 44 mm . The geometrical concentration is $C_{\text{geo}} = 1000$ [15], [17].

The manufacturing process is described in [17]. One module includes 690 cells, hence 2921 cells/m^2 . The required alignment accuracy was determined by using an in-house ray tracing tool Raytrace3D [18], developed at Fraunhofer ISE. We simulate the optical losses (light hitting the solar cell) of a micro-CPV cell lens unit, detailed description is shown in [17] and [18]. An acceptable optical loss through the solar cell displacement is $0.1\%_{\text{abs}}$, which leads to a required accuracy of $\pm 16.6 \mu\text{m}$.

For precise solar cell mounting, surface tension-driven self-alignment, also known as capillary self-alignment [19] is foreseen. During the heating process, the solder melts and the surface tension of the liquid solder pulls the die into perfect alignment with the underlying pad to minimize the surface energy.

It should be noted that this assembly process only requires one step of chip assembly (chip-on-board technology). This contrasts with other micro-CPV approaches based on a chip scale package approach, that require first the assembly of chip scale packages similar to LED fabrication, and second their respective assembly onto the baseplate [4], [8].

For our micro-CPV cell assembly, the receiving pad always needs a connected track for electrical connection. Moreover, polymer-based solder masks cannot be directly applied (e.g., by inkjet printing) to define the receiving pad, as they need to withstand concentrated sunlight in case of tracking errors.

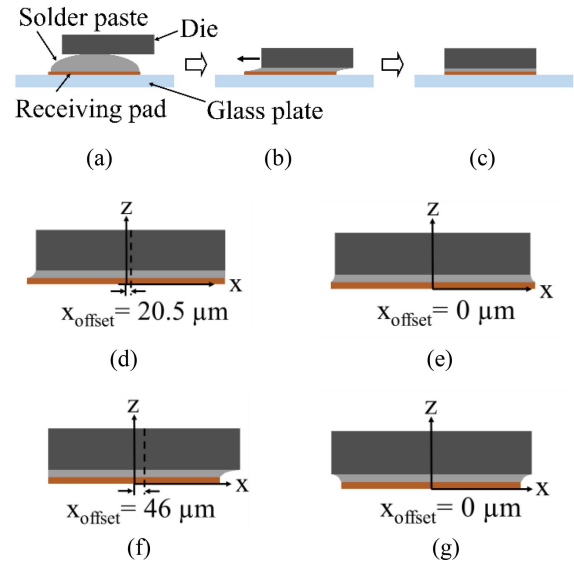


Fig. 3. (a)–(c) Process steps of self-alignment of a die on a receiving pad using the surface tension of liquid solder for the case of shape matching. (d)–(g) Illustrations of different scenarios: edge- and center-aligned dies on a larger or smaller pad (sizes to scale with respect to the experiments performed in this article). (a) Inaccurate die placement. (b) Liquid solder wets pad and die surface, surface tension forces act on the die. (c) Cooling down and solder freezing after self-alignment. (d) Pad > die: Edge alignment. (e) Pad > die: Center alignment. (f) Pad < die: Edge alignment. (g) Pad < die: Center alignment.

So far, there has been no experimental investigation of the self-alignment of a fully metalized die on a receiving pad with connected tracks and without a solder mask.

In this article, first, we investigate experimentally how manufacturing tolerances, i.e., size deviations in rectangular receiving pads, influence the accuracy of the alignment. Next, connected circuit tracks are added and the influence of solder volumes is studied for initial die to pad displacements up to $150 \mu\text{m}$. Application limits regarding solder volume and initial displacement are evaluated in detail in the Appendix.

II. MECHANISMS OF SELF-ALIGNMENT

The self-alignment process includes three steps, as depicted in Fig. 3(a)–(c). First, the die is imperfectly placed on a receiving pad equipped with a solder paste depot [see Fig. 3(a)]. The typical SAC paste is a mixture of beads of a tin-silver-copper alloy and flux and keeps the die temporarily in place. Next, during the heating process, the solder paste melts and wets the attached surfaces of receiving pad and rear side of the die. It forms a meniscus whose forced capillary action tends to align the die to the receiving pad [see Fig. 3(b)]. The main force for the die movement is originating from the surface tension of the liquid solder. The die stops when the liquid reaches the minimal surface energy or if the friction force gets equal or larger as the restoring force [see Fig. 3(c)]. If the receiving pad is larger or smaller than the die, then typically the self-alignment range is between the alignment on the left edges and on the right edges [19]. Fig. 3(d) and (f) shows edge alignment for a larger and a smaller pad than die after initial displacement in x -direction. Fig. 3(e) and (g) shows center-to-center alignment. Edge alignment leads to an offset of half of the pad to cell length difference $\pm \Delta l/2$.

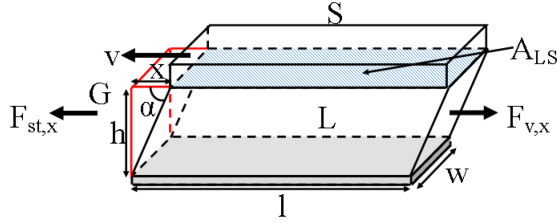


Fig. 4. Simplified sketch, sizes not to scale. The die (S) is displaced by the distance x on a liquid depot (L) with the height h . A_{LS} is the contact area of the rear side. α is the angle between the gaseous (G) and liquid (L) phase. The die moves with the velocity v .

The movement of the die can be equivalently described by either surface energy- or force-based models [19], [20], [21].

For a rectangular die with the die-liquid boundary area on the die rear side, the acting forces in lateral direction are the surface tension force F_{st} and the dynamic friction force F_v . In vertical direction pressure related force and gravity force are acting. For self-alignment the acting forces in lateral direction are relevant.

In a gaseous-solid-liquid (G-S-L) phase system, the balance between the surface tensions γ_{SG} , γ_{LS} , and γ_{LG} and the contact angle θ can be described by Young's equation (1). The resulting force acts on the contact line of the three-phase system and can be calculated by integrating along the contact lines (2).

$$\gamma_{SG} = \gamma_{LS} + \gamma_{LG} \cos \theta \quad (1)$$

$$\vec{F}_{st} = \sum_i^{LS, LG, SG} \int \gamma_i d\vec{l} \quad (2)$$

A simplified case is shown in Fig. 4, here a rectangular die with the same shape as the pad with the length l and the width w is displaced in x direction. The solder depot with the height h is simplified with straight flanks and it is assumed perfect wetting of the rear side of the die and the surface of the pad. Thus, no surface tension gradients occur on the liquid-solid interface and can be neglected. The lateral restoring force along x can be described according to (3) [19]

$$\vec{F}_{st,x} \approx 2\gamma_{LG}w \cos(\alpha) \approx 2\gamma_{LG}w \frac{x}{\sqrt{x^2 + h^2}}. \quad (3)$$

The force against self-alignment is the dynamic friction force F_v between the liquid and the solid phases, which mainly originates from the viscosity η_L of the liquid solder. This can be described by the Newton (4) [20]. The speed of the molten solder v can be set equal to the speed of the die and as the die moves with the molten solder the surface of the die rear side A_{LS} has to be taken into account [20] Klicken oder tippen Sie hier, um Text einzugeben.. Thus, the dynamic friction force in x -direction can be expressed as

$$\vec{F}_{v,x} = \eta_L A_{LS} \frac{\Delta v}{h}. \quad (4)$$

Thus, the self-alignment process is influenced by the wetting behavior of the receiving pad and die surface, the properties of the liquid, surface tension and viscosity, and the shape of dies and receiving pads, as well as the initial displacement [19].

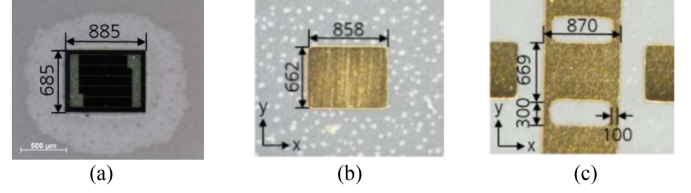


Fig. 5. Microscope pictures of the different materials. All sizes are in μm . (a) Solar cell. (b) Rectangular pad R_B . (c) Interconnected rectangular pad I .

Previous studies have analyzed the influence of the liquid volume on the self-alignment process [22], [23]. It is noted that the reflow conditions and alloy composition can have an additional influence [24]. Regarding the solder volume, there exists an optimum amount between too less and too much volume [22]. With insufficient volume, the receiving pad and die surfaces are not completely wetted. Therefore, the die can touch the substrate and resulting dry friction can prevent accurate alignment [22]. On the contrary, too much solder volume increases the risk of a tilted and misaligned chip [22], [25].

The influence of the receiving pad layout on the die alignment accuracy was also investigated using water droplets [22], [23] and solder paste [20], [24]. Conventional SMDs are typically mounted on two receiving pads [20], [24]. There, for the electrical interconnection, one track is connected to one receiving pad, and is covered with solder mask. Härter [24] investigated different layouts of two receiving pads per die (SMD type 01005) like different circle sizes, rectangular sizes but also special shapes. In general, self-alignment worked for all layouts, but the highest accuracy with the most robust process was reached for two pads with a rectangular shape, matching with the shape of the device. Smaller or larger rectangular shapes than device size increased the scattering.

Other layouts like regular hexagons, squares, rectangles and circles, but also without in-plane rotational symmetry like semi-circles and commas, were investigated with water droplets [23]. The dies were rectangular with a pattern on the backside, corresponding to the receiving pad. Self-alignment worked for all in-plane rotational symmetric shapes, but approximately for 30–40% for pads without in-plane rotational symmetry.

If the die has the same shape as the receiving pad and just the size differs, it can lead to partial self-alignment, corner self-alignment or edge self-alignment [19]. In summary, it is beneficial, if the layouts of the receiving pad and die are matching, size differences lead to higher scatterings [23], [24].

III. MATERIAL AND METHODS

A. Materials: Solar Cells and Receiving Pad Layouts

Micro-solar cells with a footprint of $885 \times 685 \mu\text{m}^2$ and thickness of $190 \mu\text{m}$ are placed on different solder depots on receiving pads with different layouts [see Fig. 5(a)].

The receiving pads are fabricated by a subtractive PCB process and consist of $30 \mu\text{m}$ copper with a chemical nickel/gold finish on a 3 mm thick glass substrate. Three rectangular pads ("R"), i.e., freestanding pads without connected tracks [see

TABLE I
SIZES OF THE RECEIVING PADS

Layout	Shape	$\Delta(\text{pad-cell})$ length [μm]	$\Delta(\text{pad-cell})$ width [μm]
R_A	Rectangular	-92 ± 2.5	-89 ± 3.0
R_B	Rectangular	-27 ± 3.2	-23 ± 3.3
R_C	Rectangular	$+41 \pm 4.2$	$+44 \pm 2.5$
I	Interconnected rectangular pad	-15 ± 2.1	-16 ± 2.1

TABLE II
OPENING SIZES OF THE STENCIL MASK, THE MEASURED SOLDER
THICKNESSES AND VOLUMES

Opening	1	2	3	4
Opening size [μm^2]	615x454	665x491	715x528	765x565
Measured solder thickness R_B [μm]	28.1 ± 3.2	35.3 ± 4.5	40.1 ± 2.6	50.9 ± 5.4
Measured solder thickness I [μm]	5.3 ± 3.2	7.1 ± 4.8	8.0 ± 5.0	15.4 ± 4.3
Solder volume (solid state) [nl]	16	20	23	29

Fig. 5(b)], of different sizes as well as one interconnected pad (“ I ”) with connected tracks [see Fig. 5(c)] are investigated. The nominal pad sizes were designed to be equal and $65 \mu\text{m}$ smaller and larger than the cell edge lengths. However, the subtractive PCB process yielded approximately $30 \mu\text{m}$ smaller. The actual pad to cell deviations are given in Table I.

B. Assembly Process

The assembly process including stencil printing and die assembly took place at CEA-Leti. First, the pads are cleaned with first acetone and then ethanol to create a comparable surface condition and increase the surface energy, especially the dispersive part. Afterwards, $\text{Sn}_{96.5}\text{Ag}_{3.0}\text{Cu}_{0.5}$ solder paste with a flux content of $11.5 \pm 1.0\%$ and particle sizes between 20 and $45 \mu\text{m}$ is applied using stencil printing. Due to the flux and the particles, a reduction of solder volume is expected after melting. To control the solder volume, the rectangular openings of a $200 \mu\text{m}$ thick stencil mask are varied from $615 \times 454 \mu\text{m}^2$ to $765 \times 565 \mu\text{m}^2$ (see Table II). The layout was designed according to IPC-7525B stencil design guidelines to achieve solder thicknesses between 40 and $85 \mu\text{m}$, assuming 50% shrinkage. The cells are assembled with pick-and-place tool with a $< 5 \mu\text{m}$ accuracy. Here, the cells are intentionally ideally placed ($\Delta x_{\text{initial}} = 0 \mu\text{m}$) or displaced with respect to the receiving pad position, with center-to-center displacements of $\Delta x_{\text{initial}} = 50, 100, \text{ and } 150 \mu\text{m}$. Reflow solder melting is performed with a comparatively slow heating ramp up to $255 \text{ }^\circ\text{C}$, resulting in 2.5 min above the liquidus temperature of $217 \text{ }^\circ\text{C}$. The resulting thickness of the solder depends on the pad sizes: for layout R_B the resulting solid solder thickness is between 28.1 and $50.9 \mu\text{m}$ and for layout I between 5.3 and $15.4 \mu\text{m}$. The solder volume is calculated based on the solder thickness on the pads R_B and are between 16 and 29 nl. Note, that these volumes are the solid volumes

and are assumed to be slightly larger in the liquid state. For each variation, 20 samples are prepared. After assembly, all solar cells are performing electrically as expected.

The offset of the cell center to receiving pad center Δx_{offset} after the assembly process is determined by measuring accurate x, y positions of cells and pads before and after the process (coordinate measurement device accuracy $< 2 \mu\text{m}$).

IV. RESULTS

A. Cell Alignment Accuracies on Rectangular Pads

In the following the influence of pad size, solder volume, and initial displacement on the self-alignment of dies on the rectangular pads is described.

1) *Solder Volume*: First, four solder volumes (1, 2, 3, 4) are varied for one rectangular receiving pad R_B .

Fig. 6(a) shows the offset of the cell center to the receiving pad center Δx_{offset} after the melting process as a function of the solder volume. The top graph shows the case of perfect placement of die to receiving pad, i.e., $\Delta x_{\text{initial}} = 0 \mu\text{m}$, whereas the bottom graph shows the data for a case of significant initial displacement of $\Delta x_{\text{initial}} = 150 \mu\text{m}$. Here, the pad R_B is smaller by $27 \mu\text{m}$ than the cell. The cell is expected to stop when the cell is fully placed above the smaller or larger pad. Thus, several alignments are possible, from the left edge to right edge alignment. When the cell to pad offset is within this range $\pm \Delta l/2$, shown in yellow in Fig. 6, then the self-alignment is seen to be successful. As a first observation, with ideal initial alignment, the cells move somewhat during the process, but show no preferred direction: The median offset (black) is close to the abscissa. The dark gray area represents the 25–75 percentiles (P25–P75), the light gray area the 10–90 percentiles (P10–P90). The scattering within 25–75 percentiles increases by around 82% with increased solder volume from 16 to 29 nl, which is from $-1 - +3 \mu\text{m}$ for 16 nl to $-22 - +2 \mu\text{m}$ for 29 nl. For initial displacements of $150 \mu\text{m}$ the median line follows the upper border of the self-alignment range $\pm \Delta l_B/2$, hence, cell edge to pad edge alignment. For the case with initial displacement also a noticeable reduction in the scattering is observed. For example, for 20 nl and no initial displacement the P25–P75 offsets are between -11 and $7 \mu\text{m}$, whereas for $x_{\text{initial}} = 150 \mu\text{m}$ between 13 and $22 \mu\text{m}$.

2) *Rectangular Pad Size*: The second part of the study investigates the influence of pad size. Here, for one solder volume, three different rectangular pad sizes (R_A, R_B, R_C) are evaluated (see Table I).

Fig. 6(b) shows for the three different pad sizes (R_A, R_B, R_C) the offsets of cells to pads Δx_{offset} as a function of initial displacements $\Delta x_{\text{initial}}$ for the solder volume of 20 nl. For the smallest pad R_A , which is $92 \mu\text{m}$ smaller than the cell, independent of the initial displacement all data scatters around a median offset close to zero with offsets $\Delta x_{\text{offset}} \leq 7.5 \mu\text{m}$. When the pad size is closer to the size of the die, R_B $27 \mu\text{m}$ smaller than the die (middle) and R_C $41 \mu\text{m}$ larger than the die (bottom) the data shows a different picture: The scattering of the data is significantly larger with offsets up to $31.1 \mu\text{m}$. Interestingly, for small initial displacements the scattering is

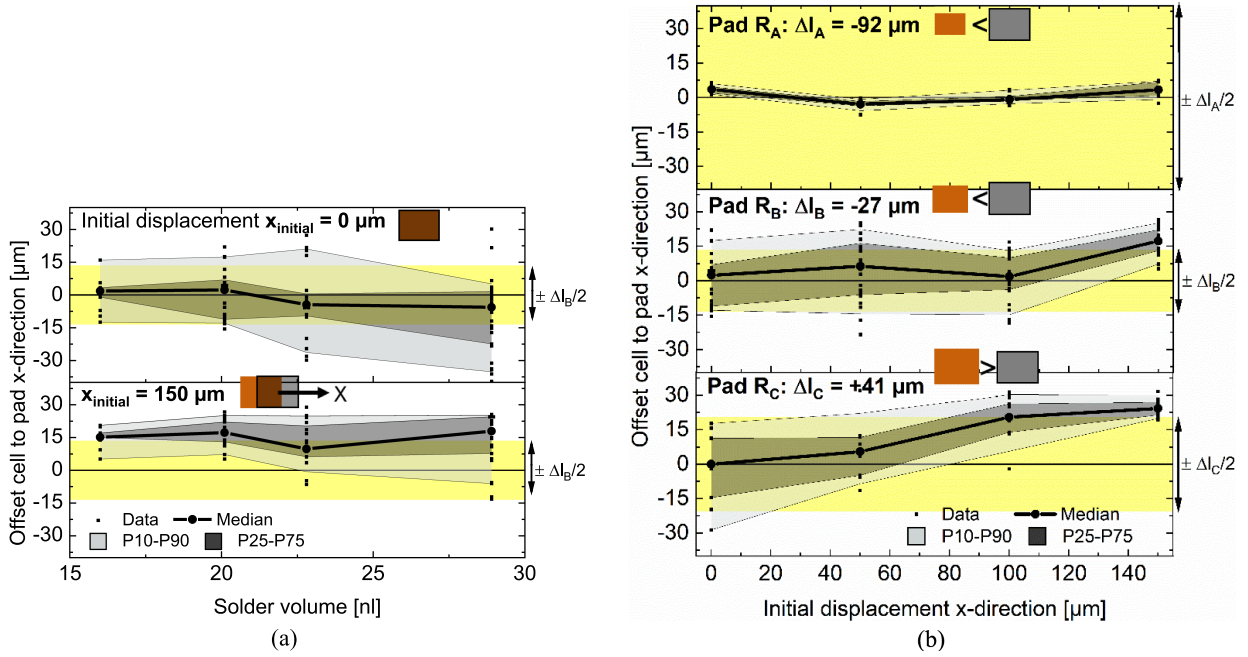


Fig. 6. Offset in x -direction of the cell to a rectangular pad Δx_{offset} as a function of (a) solder volume with pad layout R_B for the cases of ideal alignment ($\Delta x_{\text{initial}} = 0$, a-top) and for an initial displacement of $\Delta x_{\text{initial}} = 150 \mu\text{m}$ (a-bottom). The second graph (b) plots Δx_{offset} as function of the initial displacement $\Delta x_{\text{initial}}$ for the case of a solder volume of 20 nl. From top to bottom the pad size, difference pad to cell length, is varied from $\Delta I_A = -92 \mu\text{m}$ to $\Delta I_B = -27 \mu\text{m}$ to $\Delta I_C = +41 \mu\text{m}$. The yellow area visualizes the self-alignment range $\pm \Delta I/2$, the dark gray area the offsets within 25–75 percentiles, light gray 10–90 percentiles and the thick black line the median offset. (a) Pad layout R_B $\Delta I_B = -27 \mu\text{m}$. (b) Solder volume 20.1 nl.



Fig. 7. Microscope images of cells placed on receiving pad I with a solder volume of (a) 16 nl and (b) 29 nl after reflow melting. For all solder volumes the solder flows along the tracks.

rather isotropic and the median close to zero. However, for displacement above $100 \mu\text{m}$ the data shifts upward and scatters around a median at the upper border of the self-alignment range $\pm \Delta I/2$, again shown in yellow. At the same time, with increasing initial displacement, the scattering reduces, namely the P25–P75 range by 49.6% for pad layout R_B and by 78.3% for pad layout R_C over the investigated range.

B. Cell Alignment Accuracies on Pads With Connected Circuit Tracks

In micro-CPV, the electrical interconnection requires that the receiving pads need at least on one side a track connected to them. In this article, we investigate the influence of the connected tracks for the interconnected pad design I , four different solder volumes between 16 and 29 nl (see Table II) and different initial displacements up to $150 \mu\text{m}$.

For all four volumes, solder flows along the circuit tracks (see Fig. 7). Therefore, the solder layer thickness reduces to between

5 and $15 \mu\text{m}$, and therefore is significantly lower than on the rectangular pads.

Fig. 8 plots the measured offsets in x - and y -direction, (a) Δx_{offset} and (b) Δy_{offset} , against solder volume for different initial displacement between $0 \mu\text{m}$ and $150 \mu\text{m}$ (top to bottom). The x -direction is defined as perpendicular to the connected circuit track, whereas the y -direction is along it. Note that the cells here are also initially displaced in the two different directions, i.e., (a) shows data with varying Δx_{offset} but for $\Delta y_{\text{offset}} = 0$, whereas for (b) it is vice versa. The range of the percentiles P10–P90 and P25–P75 as well as the self-alignment range are illustrated in the graphs analogous with Fig. 6.

In general, for displacements in x -direction [see Fig. 8(a)] the median is close to zero for all cases and no clear trends are observed, expect for a slight reduction in the scattering when the initial displacement is introduced (i.e., for $\Delta x_{\text{initial}} > 0$).

In contrast, for cell to pad displacements in y -direction, increasing solder volume leads to increased scattering in the cell position after self-alignment. However, with increasing initial displacement $\Delta y_{\text{initial}}$ this effect reduces. The median offsets do not follow a clear trend. Finally, the scattering in y -direction is observed to be higher by 46% on average than in x -direction for the same initial displacement and the same volume.

V. DISCUSSION

A. Cell Alignment Accuracies on Rectangular Receiving Pads

1) *Solder Volume*: In general, we observed for all rectangular receiving pads that the scattering of the cell to pad offsets increases with increased solder volume.

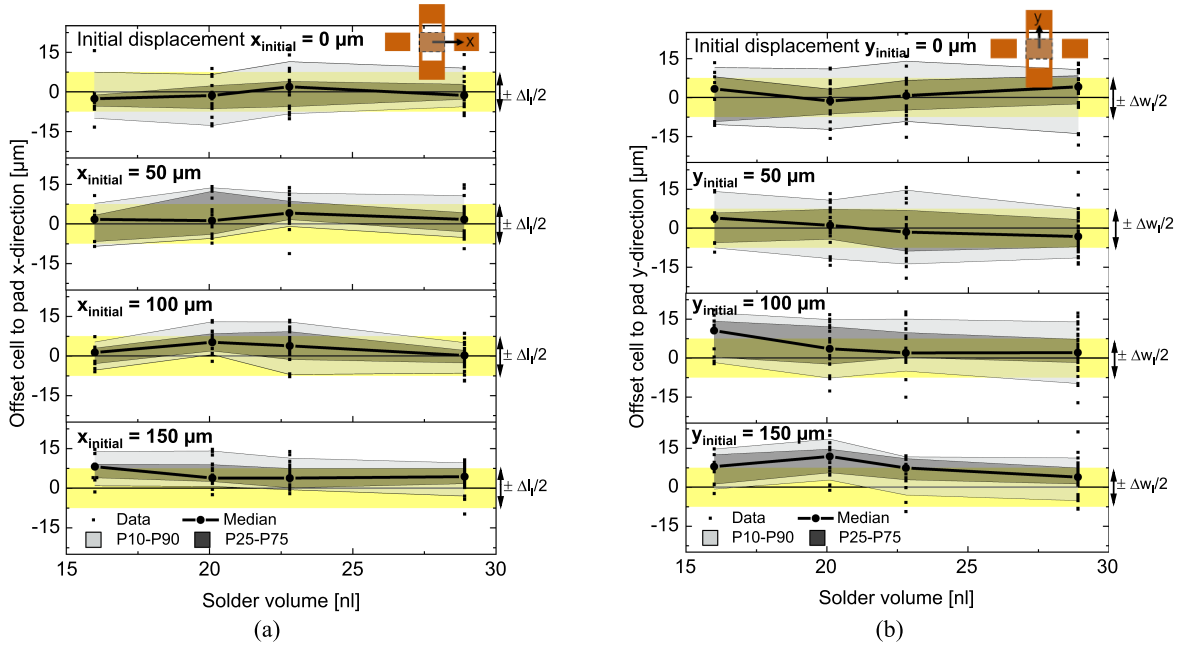


Fig. 8. (a) and (b) Offset of the cell to receiving pad I dependent on solder volume for initial displacement (a) in x -direction and (b) in y -direction. From top to bottom: Initial displacement x_{initial} or y_{initial} is increased from 0 to 150 μm . The median offset (black line) is for nearly all cases in the self-alignment range $\pm \Delta l_I/2$ or $\pm \Delta w_I/2$ (yellow). Note, that the solder volume is given as the volume applied to the pad. Here, the solder layer thickness is significantly reduced by solder leaving the target pad area. Note, the y -scale differs compared to Fig. 6. (a) Pad layout $I \Delta l_I = -15 \mu\text{m}$. (b) Pad layout $I \Delta w_I = -16 \mu\text{m}$.

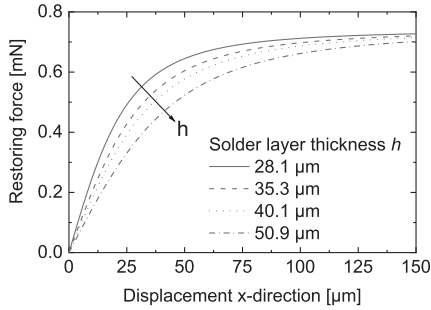


Fig. 9. Calculated restoring force according to (3) as function of the displacement of a die on the pad layout R_B and for different solder layer thicknesses. Surface tension of the molten solder $\text{Sn}_{96.5}\text{Ag}_{3.0}\text{Cu}_{0.5}$ is set to 0.54 $\text{N}\cdot\text{m}$ [26].

Larger solder volume implies larger solder layer thickness h , which according to (3), reduces the restoring force ($\sim x/\sqrt{x^2 + h^2}$). However, the dynamic friction force, acting against the restoring force, also decreases with a higher cell to pad distance ($\sim \Delta v/h$), see (4). The dynamic friction force is constant over all displacements given under the assumption of constant velocity. To evaluate the magnitude of the dynamic friction force we can estimate a velocity of 0.1 m/s and for the case of the lowest solder layer thickness we get a dynamic friction force of 0.004 mN. In comparison, the restoring force is higher for larger displacements and gets closer to zero with smaller displacements. Fig. 9 shows the curve for the four investigated solder layer thicknesses of the pad layout R_B dependent on the displacement of the die. The restoring force is equal to 0.004 mN for $x < 0.3 \mu\text{m}$. Thus, in the investigated case, the restoring force is dominating for nearly all displacements.

In more detail, for large offsets ($x \gg h$) the influence of the solder thickness on the restoring force diminishes ($\sim 1/x$), whereas for small offsets ($x \ll h$) the thickness is important $\sim x/h$. Here, the initial displacements are up to 150 μm and the solder thicknesses h between 28 and 56 μm . Thus, they differ by only half an order of magnitude at the maximum. However, the dependency of the restoring force on the solder volume is valid. For example, for a displacement of 30 μm the restoring force differs between the minimal and maximal solder layer thickness by 29.6% whereas for a displacement of 100 μm the restoring force differs by 7%. The increased dependency on the solder thickness for small offsets fits to the observed behavior, as for all performed experiments offsets remained below 30 μm , despite initial displacements between 50 and 150 μm .

2) *Rectangular Pad Size:* Our study showed that for the case of rectangular receiving pads which are significantly smaller than the dies (R_A), typically cell center to pad center alignment occurs. This was observed independent of the initial displacement [see Fig. 6(b)]. For rectangular pads only slightly smaller (R_B) or larger (R_C) than the die, for small displacements the dies scatter rather isotropic around zero but tend to edge alignment for larger initial displacements.

For dies on smaller or larger pads, center to center or edge alignment occurs depending on the balancing forces. The motion of the die stops when the restoring force either becomes zero or equal or lower to an opposed friction force. According to (3), the restoring force depends on the cell edge to pad edge distance. In the case of edge alignment, the restoring force on the side where the die aligns at the edge is zero, whereas on the opposite side it still depends on the cell edge to pad edge distance. If the pad is significantly smaller than the cell, the restoring force is

higher than for slightly smaller or larger pads. Fig. 3(d) and (f) illustrates the dimensions to scale for the pads R_C and R_A . It has to be noted that (3) is a simplification and to explain the self-alignment behavior more accurate, numerical simulations are required, which is in preparation [27].

Furthermore, for the slightly smaller and larger rectangular pads R_B and R_C , for no initial displacement the median offsets are close to $0 \mu\text{m}$ whereas for higher initial displacement the median offsets are close to the border of the self-alignment range $\pm\Delta/2$ and thus edge aligned. Additionally, for the case of ideal placement with no initial offset the scattering is higher than for the cases of nonzero initial displacements. When the cell is accurately placed, there is no force which induces a motion. When the cell is initially displaced, the initial restoring force increase with increasing offset. It seems that at the edge of the pad the restoring force is as high as the friction force and the cell stops. It should be noted, that even for the case of ideal initial placement some scattering is observed. To some extent the cause for this scattering could simply be machine precision and measurement uncertainty. Yet, some deviations are larger than those which suggests that additional effects can have a minor impact. These could possibly be from nonideal surface wetting, the transport from the pick and place tool to the reflow oven or vibration of the conveyor belt during the reflow process.

It is important to emphasize that the solder volume for all pad sizes were constant. Hence, the solder layer thickness differs, namely for a solder volume of 20 nl by $12.8 \mu\text{m}$ between the smallest (R_A) and the largest (R_B) pad. Still, the previous finding that a thinner solder layer is beneficial does not apply here, because presumably the influence of the pad size dominates the behavior.

3) *Receiving Pad Layout With Connected Tracks*: Receiving pads with connected tracks showed a different behavior regarding the influence of initial displacements and solder volumes compared to rectangular receiving pads with no connected tracks.

The receiving pad with connected tracks allows solder flowing along the tracks. Therefore, the solder layer thinned down by a factor between 3.3 and 5.3, compared with the rectangular pad R_B . This leads to two different effects: First, the solder layer thickness varies between 5.3 and $15.4 \mu\text{m}$. Thus, the dependency on the solder layer thickness decreases and an even scattering of the offsets is to be expected. For classification, for the rectangular pad R_B the difference in the offset scattering between the two lowest thicknesses, 28 and $35 \mu\text{m}$, was in the P10–P90 range between 6 to 14% dependent on the initial displacement. Hence, dependencies below this range are expected for lower thicknesses. Second, the solder flow along the tracks, even for the case of ideal placement, causes a stronger motion than with the isolated rectangular pad. This motion leads to overcoming the static friction force and thus, all cell to pad offsets are similar independently of the initial displacement.

Regarding the direction of the self-alignment, initial displacement in y -direction lead to slightly higher scattering than for initial displacements in x -direction. This is understood as a result of the tracks which partially cover the backside of the cell and thereby reduce the restoring force. Yet, it is noted that despite

this reduction of the restoring force, self-alignment still occurs for all cells.

VI. CONCLUSION

We have experimentally investigated the influence of three different rectangular receiving pad layouts, one receiving pad with connected circuit tracks, four different solder volumes, and different initial cell displacements on the self-alignment accuracy of micro-solar cells. For isolated rectangular receiving pads without connected circuit tracks, a significantly smaller pad than cell, here R_A , smaller by $92 \mu\text{m}$ than the die, compared to slightly smaller (R_B by $-27 \mu\text{m}$) or larger (R_C by $+41 \mu\text{m}$) pads, leads to best results. Depending on the initial displacement the scattering of the offsets of R_A , compared to R_B and R_C is reduced between 47.2 and 88.8% . As a consequence, we recommend significantly smaller receiving pads than die to reach a more robust process. Most important, initial displacements of the dies lead to higher alignment accuracies and reduced scattering on rectangular pads. The reason is the motion induced by the surface tension force, i.e., the friction force is overcome. The investigated solder volumes; between 16 and 29 nl , are all sufficient for self-alignment, although lower volume results in less scattering and is, thus, recommended. For pads with connected tracks, molten solder flows along the tracks, which leads to low thicknesses and decreases the sensitivity on solder volume. Furthermore, initial displacements like for rectangular pads, are not required to reach higher alignment accuracies. Here, the motion is induced by the solder flow along the tracks, which leads already to overcoming the friction force. With self-alignment, placement accuracies for the pad I between $-15 \mu\text{m}$ and $+15 \mu\text{m}$ were reached. According to raytracing simulations, this results in optical losses below $0.1\%_{\text{abs}}$ and fulfills the required accuracy for our micro-CPV module.

APPENDIX

A. Limits of Self-Alignment

The purpose of this article was to test the limits of the self-alignment. Therefore, solder volume was largely decreased and increased as well as the initial displacement were shifted to extremes.

For initial displacement up to $500 \mu\text{m}$, which is more than half of the die width, we found that mostly self-alignment still works, but sometimes major failure modes occur, which are depicted in Fig. 10. Failure can occur due to solder flowing along the rear side of the cell to the opposite circuit track [see Fig. 10(b)]. Then, an additional surface tension force pulls in the other direction and the die is balanced between the receiving pad and the opposite track. In principle this failure mode can occur only if the die is initially displaced farther than the gap width between pad and circuit track, here $200 \mu\text{m}$, and at the same time a large solder volume is applied. If the solder volume is too low, the backside of the cell as well as the pad fail to be wetted completely [see Fig. 10(c)]. In this case, the restoring force is smaller than the friction force and the self-alignment of the die fails.

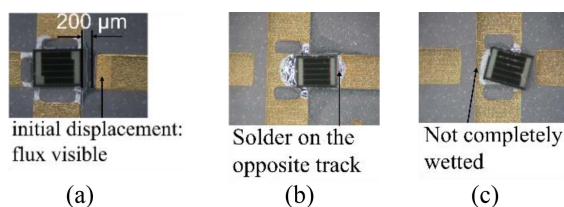


Fig. 10. Microscope images after reflow soldering. Dies placed on receiving pads with connected circuit tracks with initial displacements in x -direction of $500\ \mu\text{m}$. (a) Successful self-alignment (b) Failure: Too much solder (c) Failure: Too much solder

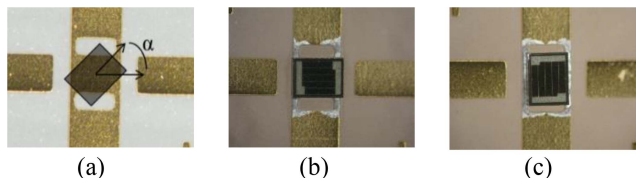


Fig. 11. Microscope images of cells soldered on receiving pad I with initial rotations. (a) Initial rotation α . (b) $\alpha < 45^\circ$, after reflow soldering. (c) $\alpha > 45^\circ$, after reflow soldering.

For asymmetric cells like the rectangular cells in this article, also the in-plane rotation of the dies is important, as illustrated in Fig. 11. For rotations below 45° the cell rotates in the preferred direction during reflow soldering, whereas for larger initial rotations, the cell rotates in the other direction. This can be relevant for self-assembly processes which are based on random motion, for example like in an automated reel-to-reel fluidic self-assembly machine [14]. In this case, symmetric squared chips would be beneficial. This is in line with the finding of Srinivasan et al. [23].

ACKNOWLEDGMENT

The authors thank P. Voarino and R. Cariou for hosting Elisa Kaiser at CEA INES and the possibility to perform the die assembly together with R. Franiatte, B. Goubault de Brugière, and D. Mermin at CEA-Leti. We thank A. Dilger at Fraunhofer ISE for support with the pick-and-place of the dies, and A. Bösch and T. Dörsam for the support in laboratory activities such as sample preparation and characterization. Furthermore, we thank P. Schöttl at Fraunhofer ISE for raytracing support. We thank our project partners EVYTRA GmbH (formerly FELA GmbH) for providing circuit boards on glass, and AZUR SPACE Solar Power GmbH for providing micro solar cell chips. The authors are responsible for the content of this article.

REFERENCES

- [1] M. Wiesenfarth, I. Anton, and A. W. Bett, "Challenges in the design of concentrator photovoltaic (CPV) modules to achieve highest efficiencies," *Appl. Phys. Rev.*, vol. 5, no. 4, 2018, Art. no. 41601.
- [2] S. Paap et al., "Cost analysis of flat-plate concentrators employing microscale photovoltaic cells for high energy per unit area applications," in *Proc. IEEE 40th Photovolt. Specialist Conf.*, 2014, pp. 2926–2929.
- [3] N. Jost, T. Gu, J. Hu, C. Domínguez, and I. Antón, "Integrated microscale concentrating photovoltaics: A scalable path toward high-efficiency, low-cost solar power," *Sol. RRL*, vol. 7, no. 16, 2023, Art. no. 2300363.
- [4] B. Furman et al., "A high concentration photovoltaic module utilizing micro-transfer printing and surface mount technology," in *Proc. 35th IEEE Photovolt. Specialists Conf.*, 2010, pp. 000475–000480.
- [5] S. Burroughs et al., "A new approach for a low cost CPV module design utilizing micro-transfer printing technology," in *Proc. AIP Conf.*, 2010, pp. 163–166.
- [6] K. Ghosal et al., "Ultrahigh efficiency HCPV modules and systems," *IEEE J. Photovolt.*, vol. 6, no. 5, pp. 1360–1365, Sep. 2016.
- [7] S. Askins et al., "Performance of hybrid micro-concentrator module with integrated planar tracking and diffuse light collection," in *Proc. IEEE 46th Photovolt. Specialists*, 2019, pp. 2507–2512.
- [8] G. Duggan et al., "ALCHEMI—A low cost, high efficiency, optoelectronic HCPV module for $1000\times$ operation," in *Proc. AIP Conf.*, 2018, Art. no. 20005.
- [9] G. Duggan et al., "Update on project ALCHEMI—A low cost HCPV module for 1000 sun operation," in *Proc. 15th Int. Conf. Concentrator Photovolt. Syst.*, 2019, Art. no. 30002.
- [10] N. Hayashi et al., "Thin concentrator photovoltaic module with micro-solar cells which are mounted by self-align method using surface tension of melted solder," *AIP Conf. Proc.*, vol. 1881, no. 1, 2017, Art. no. 80005.
- [11] C. A. Bower, E. Menard, and P. E. Garrou, "Transfer printing: An approach for massively parallel assembly of microscale devices," in *Proc. 58th Electron. Compon. Technol. Conf.*, 2008, pp. 1105–1109.
- [12] X. Sheng et al., "Printing-based assembly of quadruple-junction four-terminal microscale solar cells and their use in high-efficiency modules," *Nature Mater.*, vol. 13, no. 6, pp. 593–598, 2014.
- [13] S. Cho et al., "Micro-concentrator photovoltaics using fluidic self-assembly technology," *Adv. Mater. Technol.*, vol. 6, no. 12, 2021, Art. no. 2100312.
- [14] S.-C. Park et al., "A first implementation of an automated reel-to-reel fluidic self-assembly machine," *Adv. Mater.*, vol. 26, no. 34, pp. 5942–5949, 2014.
- [15] M. Wiesenfarth et al., "Technical boundaries of micro-CPV module components: How small is enough?," in *Proc. 17th Int. Conf. Concentrator Photovolt. Syst.*, 2022, Art. no. 30008.
- [16] P. Schroth et al., "AZUR's new 5C46 CPV cell: Final design for optimized outdoor performance," in *Proc. 17th Int. Conf. Concentrator Photovolt. Syst.*, 2022, Art. no. 20008.
- [17] E. Kaiser, P. Schöttl, M. Wiesenfarth, P. Nitz, and H. Helmers, "Effects of manufacturing tolerances on micro-CPV module performance," in *Proc. 18th Int. Conf. Concentrator*, 2023, Art. no. 30002.
- [18] P. Schöttl, G. Bern, P. Nitz, F. Torres, and L. Graf, "Raytrace3D by Fraunhofer ISE: Accurate and efficient ray tracing for concentrator optics," Fraunhofer Institut für Solare Energiesysteme ISE, Freiburg im Breisgau, Germany, 2022. Accessed: May 20, 2022. [Online]. Available: <https://www.ise.fraunhofer.de/content/dam/ise/de/downloads/pdf/raytrace3d.pdf>
- [19] M. Mastrangeli, Q. Zhou, V. Sariola, and P. Lambert, "Surface tension-driven self-alignment," *Soft Matter*, vol. 13, no. 2, pp. 304–327, 2017.
- [20] O. Krammer and Z. Illyefalvi-Vitéz, "Investigating the self-alignment of chip components during reflow soldering," *Periodica Polytechnica, Elect. Eng.*, vol. 52, no. 1-2, 2008, Art. no. 67.
- [21] P. Lambert, A. Chau, A. Delchambre, and S. Régnier, "Comparison between two capillary forces models," *Langmuir, ACS J. Surfaces Colloids*, vol. 24, no. 7, pp. 3157–3163, 2008.
- [22] K. Sato, K. Ito, S. Hata, and A. Shimokohbe, "Self-alignment of microparts using liquid surface tension—Behavior of micropart and alignment characteristics," *Precis. Eng.*, vol. 27, no. 1, pp. 42–50, 2003.
- [23] U. Srinivasan, D. Liepmann, and R. T. Howe, "Microstructure to substrate self-assembly using capillary forces," *J. Microelectromech. Syst.*, vol. 10, no. 1, pp. 17–24, 2001.
- [24] S. Härter, *Qualifizierung Des Montageprozesses Hochminiaturisierter Elektronischer Bauelemente*. Erlangen, Germany: FAU Univ. Press, 2020.
- [25] J. Berthier, K. A. Brakke, S. Mermoz, C. Frétygny, and L. Di Cioccio, "Stabilization of the tilt motion during capillary self-alignment of rectangular chips," *Sens. Actuators, A Phys.*, vol. 234, pp. 180–187, 2015.
- [26] N. Rodrigues et al., "Contact angle measurement of SAC 305 solder: Numerical and experimental approach," *J. Mater. Sci., Mater. Electron.*, vol. 27, no. 9, pp. 8941–8950, 2016.
- [27] V. Vareilles et al., "Experimental and simulative correlations of the influence of solder volume and receptor size on the capillary self-alignment of micro solar cells," *IEEE J. Microelectromech. Syst.*, to be published, doi: 10.1109/JMEMS.2024.3352396.